Digital Signal Processing 78 (2018) 250–258

Contents lists available at ScienceDirect

Digital Signal Processing

www.elsevier.com/locate/dsp

Wideband array self-calibration and DOA estimation under large position errors ☆

Yaqi Liu [a,*], Chengcheng Liu [a], Yongjun Zhao [a], Jiandong Zhu [b]

[a] Engineering National Digital Switching System Engineering and Technological Research Center, Zhengzhou, 450000, China
[b] Electronic Equipment Test Center, Luoyang, 471000, China

ARTICLE INFO

Article history:
Available online 23 March 2018

Keywords:
Wideband array self-calibration
Wideband DOA estimation
Time-frequency distributions
Propagation delays estimation

ABSTRACT

For wideband array signals, existing self-calibration methods use a first order approximation to simplify the estimation procedure under the assumption of small sensor position errors. However, the performance will degrade severely as the position errors increase. In this paper, a novel self-calibration method based on the time-frequency distributions (TFDs) is proposed to relieve the small errors constraint. We firstly develop an approach for wideband signals to select the TFDs of each source. Then the TFDs are utilized to obtain the propagation delays, which have a simple linear relationship with the sensor positions. The direction of arrival (DOA) and positions are finally estimated by a two-step iteration without any approximation. Simulation results demonstrate that the proposed method can achieve accurate DOA and position estimation over a broad range of position errors with lower computational complexity, and outperforms existing self-calibration algorithms.

1. Introduction

An important application of sensor array is to estimate the direction of arrival (DOA), and most existing DOA methods can work effectively with the exact formulation of array manifold [1,2]. However, in practice, the performance may be seriously deteriorated by gain/phase errors, sensor position errors and mutual coupling errors [3–5], among which a small perturbation in sensor position can often dominate all other errors [6]. Hence it is crucial to calibrate the array shape.

There are a number of array shape calibration methods, which can be classified into self-calibration and pilot-calibration. Self-calibration is always preferred since it does not require any known sources but relies entirely on the targets of opportunity. In [7], Rockah and Schultheiss gave the identifiability condition of self-calibration: an accurate self-calibration may be achieved for a non-linear array with sensor position errors, provided that one sensor position and the direction to a second sensor are known and three distinct sources impinge on the array. In [8] and [9], under small errors assumption, Weiss and Friedlander used a first order approximation to the sensor position parameters to simplify the estimation procedure based on conditional maximum likelihood (CML) and multiple signal classification (MUSIC), respectively. However, the approximation is not adequate under large errors. Then Flanagan and Bell proposed a method without approximations and relieved the small errors constraint [10], but it is just suitable for narrowband signals. Using particle swarm optimization (PSO), Wan and Chung carried out an algorithm based on unconditional maximum likelihood (UML) estimator [11], which achieved good performance for both narrowband and wideband signals under large errors. However, to achieve accurate estimation, the number of initial particles must be large enough, which results in huge computational complexity. It is not easy to realize the stochastic global optimization on FPGA or DSP. Hence we may prefer an algorithm without stochastic global optimization in practice.

Motivated by these facts, we propose a wideband array self-calibration and DOA estimation method under large position errors based on the time-frequency distributions (TFDs). TFDs have been used in many blind source separation (BSS) algorithms [12–15] and narrowband DOA estimation algorithms [16–18]. For signal model mismatch, these algorithms cannot be applied to wideband case. In [19,20], wideband DOA estimation based on TFDs was achieved with the precise array manifold, but it has poor robustness to position errors. In this paper, the TFDs are utilized to estimate the propagation delays of wideband signals, with which the DOAs and sensor positions can be estimated by a two-step iteration without approximations or stochastic global optimization due to the simpler relationship between the propagation delays and parameters.

☆ Funding: This work was supported by the National Natural Science Foundation of China [grant numbers 61401469].

* Corresponding author.
E-mail address: yuyang911026@163.com (Y. Liu).

https://doi.org/10.1016/j.dsp.2018.03.013
1051-2004/

Simulation results illustrate that the proposed method can provide satisfactory performance, and it has lower computational complexity.

This paper is organized as follows. In Section 2, we formulate the problem of interest by introducing the wideband array signal model and conventional self-calibration method briefly. Then an approach based on TFDs is proposed to obtain propagation delays, and the DOAs and sensor positions are estimated by a two-step iteration in Section 3. In Section 4, the algorithm analysis is given. The performance of the proposed method is examined by the simulation results in Section 5. Conclusions are finally drawn in Section 6.

2. Problem formulation

2.1. Signal model

Consider K wideband signals $s_k(t)$ $(k = 0, 1 \ldots, K-1)$ impinging on a nonlinear array of M $(M \geq K)$ sensors, and denote $x_m(t)$ $(m = 0, 1, \ldots, M-1)$ as the received signal. Then the far-field signal model can be written as

$$x_m(t) = \sum_{k=0}^{K-1} s_k(t - \tau_{k,m}) + n_m(t) \quad m = 0, 1, \ldots, M-1 \tag{1}$$

where $\tau_{k,m}$ is the propagation delay of $s_k(t)$ from mth sensor to the reference sensor, and $n_m(t)$ denotes the additive noise. In the presence of position errors, $\tau_{k,m}$ is written as

$$\tau_{k,m} = \frac{\cos(\theta_k)(x_m + \Delta x_m) + \sin(\theta_k)(y_m + \Delta y_m)}{c} \tag{2}$$

in which θ_k is the DOA of s_k, x_m and y_m are the nominal x and y positions of the mth sensor, and the corresponding position errors are Δx_m and Δy_m. c is the speed of propagation. Here the sensors and sources are assumed coplanar to simplify the expression like existing methods [6–11].

Equation (1) can be rewritten in vector form as

$$\boldsymbol{x}(t) = \sum_{k=0}^{K-1} \boldsymbol{s}_k(t) + \boldsymbol{n}(t) \tag{3}$$

where $\boldsymbol{x}(t) = [x_0(t), x_1(t), \ldots, x_{M-1}(t)]^T$ is the received signal vector with the superscript $(\cdot)^T$ denoting the transpose operator. $\boldsymbol{s}_k(t) = [s_k(t - \tau_{k,0}), s_k(t - \tau_{k,1}), \ldots, s_k(t - \tau_{k,M-1})]^T$ is the kth source signal vector. $\boldsymbol{n}(t) = [n_0(t), n_1(t), \ldots, n_{M-1}(t)]^T$ is the noise vector.

Our primary goal is to estimate the DOAs. However, it can be hardly achieved under position errors. Hence the sensor positions also need to be estimated accurately. In [7], it is shown that simultaneous DOAs and positions estimation is possible provided that the sensor array is not linear and there are three distinct sources as well as knowledge of the exact position of one sensor and the direction to a second sensor. Without loss of generality, we assume that the position of first sensor and the y position of the second sensor are known as $x_0 = 0$, $y_0 = 0$ and $y_1 = 0$. Under this assumption, one effective method suitable for wideband signals is the method in [9]. It is referred to as WF method and reviewed briefly as follows.

2.2. WF method under small position errors

Under small position errors, WF method iterates between two steps: the first step assumes known sensor positions and estimates the DOAs, then the second step assumes known DOAs and estimates the sensor positions.

The first step: Given the initial or the last estimated sensor positions, the DOAs are estimated from K largest peaks in the MUSIC spectrum

$$P_{\mathrm{MU}}(\theta) = \frac{1}{\sum_{l=1}^{L} \|\hat{\boldsymbol{U}}_N^H(f_l)\boldsymbol{a}(f_l, \theta)\|^2} \tag{4}$$

where $\boldsymbol{a}(f_l, \theta) = [e^{-j2\pi f_l \tau_0}, e^{-j2\pi f_l \tau_1}, \ldots, e^{-j2\pi f_l \tau_{M-1}}]^T$ is the steering vector at frequency f_l, and $\tau_m = [\cos(\theta)\hat{x}_m + \sin(\theta)\hat{y}_m]/c$ $(m = 0, 1, \ldots, M-1)$ denotes the propagation delay corresponding to θ. $\hat{\boldsymbol{U}}_N(f_l) = [\boldsymbol{u}_K(f_l), \boldsymbol{u}_{K+1}(f_l), \ldots, \boldsymbol{u}_{M-1}(f_l)]$ is the noise subspace of $\boldsymbol{R}_{\boldsymbol{x}}(f_l) = E[\boldsymbol{x}(f_l)\boldsymbol{x}^H(f_l)]$ where $\boldsymbol{x}(f_l)$ is the frequency f_l component of the received signal. $\boldsymbol{u}_K(f_l), \boldsymbol{u}_{K+1}(f_l), \ldots, \boldsymbol{u}_{M-1}(f_l)$ are the $M-K$ eigenvectors of $\boldsymbol{R}_{\boldsymbol{x}}(f_l)$ corresponding to the smallest $M-K$ eigenvalues. L is the number of selected frequencies. $\|\cdot\|$ and $(\cdot)^H$ stand for the Frobenius matrix norm and Hermitian transpose, respectively.

The second step: With the DOAs $\hat{\theta}_0, \hat{\theta}_1, \ldots, \hat{\theta}_{K-1}$ estimated by the first step, the position errors $\Delta\boldsymbol{x} = [\Delta x_0, \ldots, \Delta x_{M-1}]^T$ and $\Delta\boldsymbol{y} = [\Delta y_0, \ldots, \Delta y_{M-1}]^T$ can be obtained by maximizing the following cost function

$$P_{\mathrm{MU}}(\Delta\boldsymbol{x}, \Delta\boldsymbol{y}) = \frac{1}{\sum_{l=0}^{L-1} \|\hat{\boldsymbol{U}}_N^H(f_l)\boldsymbol{A}(f_l)\|^2} \tag{5}$$

where $\boldsymbol{A}(f_l) = [\boldsymbol{a}(f_l, \hat{\theta}_0), \boldsymbol{a}(f_l, \hat{\theta}_1), \ldots, \boldsymbol{a}(f_l, \hat{\theta}_{K-1})]$ is the steering matrix at f_l. If $(\Delta x_m, \Delta y_m)$ is small enough, $\boldsymbol{A}(f_l)$ can be expanded as

$$\boldsymbol{A}(f_l) = \boldsymbol{A}_0(f_l) + \boldsymbol{\Lambda}_{\boldsymbol{x}}\boldsymbol{A}_1(f_l) + \boldsymbol{\Lambda}_{\boldsymbol{y}}\boldsymbol{A}_2(f_l) \quad l = 0, 1, \ldots, L-1 \tag{6}$$

where $\boldsymbol{A}_0(f_l)$ denotes the $\boldsymbol{A}(f_l)$ calculated with the initial or the last estimated sensor positions $(\hat{x}_{m0}, \hat{y}_{m0})$, and

$$\begin{aligned}
&\boldsymbol{\Lambda}_{\boldsymbol{x}} \triangleq \mathrm{diag}\{\Delta x_0, \Delta x_1, \ldots, \Delta x_{M-1}\} \\
&\boldsymbol{\Lambda}_{\boldsymbol{y}} \triangleq \mathrm{diag}\{\Delta y_0, \Delta y_1, \ldots, \Delta y_{M-1}\} \\
&\boldsymbol{A}_1(f_l) \triangleq -j\boldsymbol{A}_0(f_l)\frac{2\pi f_l}{c}\mathrm{diag}\{\cos(\hat{\theta}_0), \cos(\hat{\theta}_1), \ldots, \cos(\hat{\theta}_{K-1})\} \\
&\boldsymbol{A}_2(f_l) \triangleq -j\boldsymbol{A}_0(f_l)\frac{2\pi f_l}{c}\mathrm{diag}\{\sin(\hat{\theta}_0), \sin(\hat{\theta}_1), \ldots, \sin(\hat{\theta}_{K-1})\}
\end{aligned} \tag{7}$$

Based on (6), we can obtain $\Delta\boldsymbol{x}, \Delta\boldsymbol{y}$ that maximize $P_{\mathrm{MU}}(\Delta\boldsymbol{x}, \Delta\boldsymbol{y})$ as

$$[\Delta\boldsymbol{x}^T, \Delta\boldsymbol{y}^T]^T = [\mathrm{Re}(\boldsymbol{Q}^H\boldsymbol{Q})]^{-1}\mathrm{Re}(\boldsymbol{Q}^H\boldsymbol{Z}) \tag{8}$$

where $\boldsymbol{Q}$ and $\boldsymbol{Z}$ are constructed as

$$\begin{aligned}
&\boldsymbol{Q} = [\boldsymbol{Q}^T(0,0), \boldsymbol{Q}^T(0,1), \ldots, \boldsymbol{Q}^T(L-1, K-1)]^T \\
&\boldsymbol{Z} = [\boldsymbol{Z}^T(0,0), \boldsymbol{Z}^T(0,1), \ldots, \boldsymbol{Z}^T(L-1, K-1)]^T
\end{aligned} \tag{9}$$

in which

$$\begin{aligned}
&\boldsymbol{Q}(l,k) = -[\hat{\boldsymbol{U}}_N^H(f_l)\mathrm{diag}\{\boldsymbol{a}_1(f_l,k)\}, \hat{\boldsymbol{U}}_N^H(f_l)\mathrm{diag}\{\boldsymbol{a}_1(f_l,k)\}] \\
&\boldsymbol{Z}(l,k) = \hat{\boldsymbol{U}}_N^H(f_l)\boldsymbol{a}_0(f_l,k)
\end{aligned} \tag{10}$$

where $\boldsymbol{a}_0(f_l,k)$, $\boldsymbol{a}_1(f_l,k)$ and $\boldsymbol{a}_2(f_l,k)$ are the kth column vectors of $\boldsymbol{A}_0(f_l)$, $\boldsymbol{A}_1(f_l)$ and $\boldsymbol{A}_2(f_l)$, respectively. Then the new positions are easily calculated as

$$(\hat{x}_m, \hat{y}_m) = (\hat{x}_{m0}, \hat{y}_{m0}) + (\Delta x_m, \Delta y_m) \tag{11}$$

The final DOAs and sensor positions are obtained by repeating the two steps above till convergence.

The WF method can achieve accurate DOAs and positions estimation under small errors, but the performance will degrade severely with the errors increasing. The main reason is that (6) does not hold under large errors, thus the positions estimated by (8) and (11) will have big biases. Hence we need to explore a method that avoids the approximation. Observing (2), if $\tau_{k,m}$ $(k = 0, 1, \ldots K-1, m = 0, 1, \ldots, M-1)$ are known, we can directly estimate DOAs and positions by the linear equation without any approximation. Hence we will develop an approach based on TFDs to estimate the propagation delay vectors $\boldsymbol{\tau}_k = [\tau_{k,0}, \tau_{k,1}, \ldots, \tau_{k,M-1}]^T$ $(k = 0, 1, \ldots, K-1)$ of wideband signals, and estimate DOAs and positions using a new two-step iteration without approximations.

3. Proposed self-calibration method under large position errors

3.1. Propagation delays estimation based on TFDs

For a signal $z(t)$, its TFDs can be obtained by the short-time Fourier transform (STFT) defined as

$$Z(t, f) = \int_{-\infty}^{+\infty} z(\tau) g(\tau - t) e^{-j2\pi f \tau} d\tau \tag{12}$$

where $g(t)$ is a window function. In this paper, $g(t)$ is selected as Hamming window

$$g(t) = \begin{cases} [0.54 - 0.46\cos(\frac{2\pi t}{T_{\max}})] & 0 \le t < T_{\max} \\ 0 & \text{else} \end{cases} \tag{13}$$

where $T_{\max}$ is the length of window.

Under assumed noise-free environment, taking STFT of (1), we have

$$X_m(t, f) = \sum_{k=0}^{K-1} S_k(t, f) e^{-j2\pi f \tau_{k,m}} \quad m = 0, 1, \ldots, M-1 \tag{14}$$

where $X_m(t, f)$ and $S_k(t, f)$ denote the TFDs of $x_m(t)$ and $s_k(t)$, respectively. Similarly, taking STFT of (3) yields

$$\boldsymbol{X}(t, f) = \boldsymbol{A}(f)\boldsymbol{S}(t, f) \tag{15}$$

where

$$\begin{aligned} &\boldsymbol{X}(t, f) = \left[X_0(t, f), X_1(t, f), \ldots, X_{M-1}(t, f)\right]^T \\ &\boldsymbol{S}(t, f) = \left[S_0(t, f), S_1(t, f), \ldots, S_{K-1}(t, f)\right]^T \\ &\boldsymbol{A}(f) = \left[\boldsymbol{a}_0(f), \boldsymbol{a}_1(f), \ldots, \boldsymbol{a}_{K-1}(f)\right] \\ &\boldsymbol{a}_k(f) = \left[1, e^{-j2\pi f \tau_{k,1}}, \ldots, e^{-j2\pi f \tau_{k,M-1}}\right]^T, \\ &\quad (k = 0, 1 \ldots, K-1) \end{aligned} \tag{16}$$

In the TF domain, a single-source point is defined as a TF point at which only one source signal contributes to the energy, while an overlapping point is a TF point at which there is an energy contribution of more than one source signals. Fig. 1 shows the TFDs of a received signal involving two source signals s_1 and s_2. Ω_1 and Ω_2 represent the sets of single-source points of s_1 and s_2, respectively, and Ψ represents the set of overlapping points.

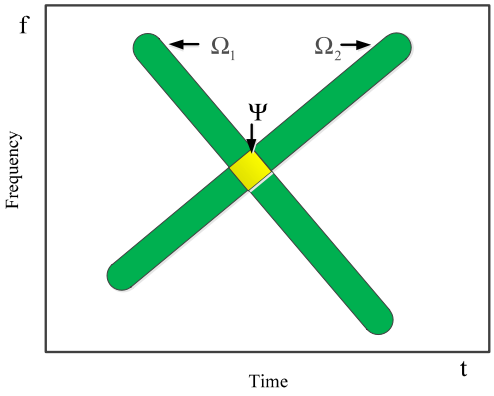

Fig. 1. TFDs of a received signal involving two source signals s_1 and s_2.

At a single-source point (t_a, f_a) of $s_k(t)$, (15) can be simplified to

$$\boldsymbol{X}(t_a, f_a) = \boldsymbol{a}_k(f_a) S_k(t_a, f_a) \quad (t_a, f_a) \in \Omega_k \tag{17}$$

where Ω_k denotes the set of single-source points corresponding to the signal $s_k(t)$. The steering vector $\boldsymbol{a}_k(f_a)$ of $s_k(t)$ at frequency f_a can be obtained by

$$\boldsymbol{a}_k(f_a) = \frac{\boldsymbol{X}(t_a, f_a)}{S_k(t_a, f_a)} \tag{18}$$

Due to $x_0 = 0$ and $y_0 = 0$, we have $\tau_{k,0} = 0$, which leads to $\boldsymbol{a}_k(f_a, 1) = 1$ and $\boldsymbol{X}(t_a, f_a, 1) = S_k(t_a, f_a)$ with $\boldsymbol{a}_k(f_a, 1)$ and $\boldsymbol{X}(t_a, f_a, 1)$ denoting the first element of $\boldsymbol{a}_k(f_a)$ and $\boldsymbol{X}(t_a, f_a)$, respectively. Then (18) can be rewritten as

$$\boldsymbol{a}_k(f_a) = \frac{\boldsymbol{X}(t_a, f_a)}{\boldsymbol{X}(t_a, f_a, 1)} \tag{19}$$

Thus, the delay vector $\boldsymbol{\tau}_k(t_a, f_a)$ can be calculated as

$$\boldsymbol{\tau}_k(t_a, f_a) = \frac{\text{unwrap}(\text{angle}(\boldsymbol{a}_k(f_a)))}{-2\pi f_a} \quad k = 0, 1, \ldots, K-1 \tag{20}$$

where unwrap$(\cdot)$ is used to correct the radian phase angles in the vector by adding multiples of $\pm 2\pi$ when absolute jumps between consecutive elements of the vector are greater than or equal to the default jump tolerance of π radians, and angle $(\boldsymbol{a}_k(f_a))$ returns the phase angles for each element of $\boldsymbol{a}_k(f_a)$.

For two different single-source points (t_{a1}, f_{a1}) and (t_{a2}, f_{a2}) of $s_k(t)$, the delay vectors satisfy

$$\boldsymbol{\tau}_k(t_{as1}, f_{as1}) = \boldsymbol{\tau}_k(t_{as2}, f_{as2}) \forall (t_{as1}, f_{as1}), (t_{as2}, f_{as2}) \in \Omega_k \tag{21}$$

where $\boldsymbol{\tau}_k(t_{as1}, f_{as1}) = \boldsymbol{\tau}_k(t_{as2}, f_{as2}) = [\tau_{k,0}, \tau_{k,1}, \ldots, \tau_{k,M-1}]^T$.

Based on (19) and (20), we can estimate the propagation delays with a single-source point. In noise environment, the estimated delay vector may have some biases, (21) suggests that we can have a more accurate estimation by averaging the delay vectors at different single-source points of the same signal. Hence a necessary task is to select the single-source points for each source signal, which can be realized by the following procedures.

1. *Noise thresholding*: Transform the received signals to the TF domain by STFT. In order to reduce the computational complexity, a noise thresholding step is then carried out to remove the points with negligible energy as following: for each time-slice (t_p, f) of the TFDs, apply (22) for all the frequency f_q points belonging to this time-slice

$$\text{if} \quad \frac{\|\boldsymbol{X}(t_p, f_q)\|}{\max_f \|\boldsymbol{X}(t_p, f)\|} \geq \varepsilon_1, \quad \text{keep } (t_p, f_q) \tag{22}$$

where ε_1 is a small threshold.

2. *TF points clustering:* After noise removing, the remaining points mainly involve single-source points and overlapping points. Calculate $\boldsymbol{\tau}(t, f)$ using (19) and (20) for all the remaining points. Based on (21), if (t_1, f_1) and (t_2, f_2) belong to the same signal, they satisfy

$$\frac{\|\boldsymbol{\tau}(t_1, f_1) - \boldsymbol{\tau}(t_2, f_2)\|}{0.5(\|\boldsymbol{\tau}(t_1, f_1)\| + \|\boldsymbol{\tau}(t_2, f_2)\|)} \leq \varepsilon_2 \tag{23}$$

where ε_2 is a small threshold. Using (23), we cluster the points into P $(P \geq K)$ classes. As shown in Fig. 1, for each source signal, the single-source points are always much more than the overlapping points, which can be easily satisfied in practice [14]. Therefore, the K largest classes Ω_k $(k = 0, 1, \ldots, K-1)$ are corresponding to the sets of single-source points for K source signals. The delay vectors can be estimated as the centroid vectors of these classes, i.e.,

$$\hat{\boldsymbol{\tau}}_k = \frac{1}{D_k} \sum_{(t,f)\in\Omega_k} \boldsymbol{\tau}(t, f), \quad k = 0, 1, \cdots, K-1 \tag{24}$$

where D_k is the number of points in Ω_k. Up to now, we have obtained the propagation delays $\hat{\tau}_{k,m}$ $(k = 0, 1, \ldots K-1,\ m = 0, 1, \ldots, M-1)$.

3.2. DOAs and sensor positions estimation

With the estimated propagation delays, the DOAs and sensor positions can be estimated by a two-step iteration without approximations.

The first step: In this step, we estimate the DOAs with the initial or the last estimated sensor positions. For each source signal, stacking (2) for $M-1$ sensors with $\hat{\tau}_{k,m}$ $(m = 1, 2, \ldots M-1,$ $\hat{\tau}_{k,0} \equiv 0$ is not utilized due to $x_0 \equiv 0$ and $y_0 \equiv 0)$ yields

$$\boldsymbol{B}\boldsymbol{\rho}_k = \boldsymbol{\varsigma}_k \quad k = 0, \ldots, K-1 \tag{25}$$

where $\boldsymbol{\rho}_k = [\cos(\theta_k), \sin(\theta_k)]^T$, $\boldsymbol{\varsigma}_k = [\hat{\tau}_{k,1}, \hat{\tau}_{k,2}, \ldots, \hat{\tau}_{k,M-1}]^T$ is a $(M-1) \times 1$ vector, and

$$\boldsymbol{B} = \frac{1}{c}\begin{bmatrix} \hat{x}_1 & 0 \\ \hat{x}_2 & \hat{y}_2 \\ \vdots & \vdots \\ \hat{x}_{M-1} & \hat{y}_{M-1} \end{bmatrix} \tag{26}$$

where $(\hat{x}_m, \hat{y}_m)$ $(m = 1, 2, \ldots, M-1)$ are the initial or the last estimated sensor positions.

We can obtain $\boldsymbol{\rho}_k$ by the least-squares (LS) method as

$$\hat{\boldsymbol{\rho}}_k = \left(\boldsymbol{B}^T\boldsymbol{B}\right)^{-1}\boldsymbol{B}^T\boldsymbol{\varsigma}_k \tag{27}$$

Since $\boldsymbol{\rho}_k = [\cos(\theta_k), \sin(\theta_k)]^T$ and $\theta_k \in [-\pi, \pi]$, θ_k is estimated as

$$\hat{\theta}_k = \begin{cases} \operatorname{arc\,cot}(\frac{\hat{\rho}_k(1)}{\hat{\rho}_k(2)}) & \hat{\rho}_k(2) \geq 0 \\ -\operatorname{arc\,cot}(-\frac{\hat{\rho}_k(1)}{\hat{\rho}_k(2)}) & \hat{\rho}_k(2) < 0 \end{cases} \quad k = 0, 1, \ldots, K-1 \tag{28}$$

where $\hat{\boldsymbol{\rho}}_k(1)$ and $\hat{\boldsymbol{\rho}}_k(2)$ denote the first and second element of $\hat{\boldsymbol{\rho}}_k$, respectively. Thus, the new DOAs are obtained.

Table 1
Wideband array self-calibration and DOA estimation based on TFDs.

Input: The nominal sensor positions and received signals
Output: Estimated DOAs and revised sensor positions

1. Calculate the TFDs of the received signal $\boldsymbol{x}(t)$ using STFT
2. Remove the noise points by (22)
3. Calculate $\boldsymbol{\tau}(t, f)$ using (19) and (20) for all the remaining points, and cluster them into P $(P \geq K)$ classes based on (23). Estimate $\hat{\boldsymbol{\tau}}_k$ using (24) with the K largest classes
4. **Repeat**
5. Estimate the DOAs using (28) with the initial or the last estimated sensors positions
6. Estimate the sensor positions using (31) with the last estimated DOAs
7. **Untill** the estimated results change slightly

The second step: In this step, the last estimated DOAs by the first step are utilized to calculate the sensor positions. Stacking (2) for all the source signals and $M-1$ sensors yields

$$\boldsymbol{H}\begin{bmatrix} \boldsymbol{\chi} \\ \boldsymbol{\gamma} \end{bmatrix} = \boldsymbol{\varsigma} \tag{29}$$

where $\boldsymbol{\varsigma} = [\boldsymbol{\varsigma}_0^T, \boldsymbol{\varsigma}_1^T, \ldots, \boldsymbol{\varsigma}_{K-1}^T]^T$, $\boldsymbol{\chi} = [x_1, x_2, \ldots, x_{M-1}]^T$, $\boldsymbol{\gamma} = [y_1, y_2, \ldots, y_{M-1}]^T$ and $\boldsymbol{H} = [\boldsymbol{H}_0^T, \boldsymbol{H}_1^T, \ldots, \boldsymbol{H}_{K-1}^T]^T$ with

$$\boldsymbol{H}_k = \frac{1}{c}\begin{bmatrix} \cos(\hat{\theta}_k) & & \sin(\hat{\theta}_k) & \\ & \ddots & & \ddots \\ & \cos(\hat{\theta}_k) & & \sin(\hat{\theta}_k) \end{bmatrix}_{(M-1)\times 2(M-1)}$$
$$k = 0, 1, \ldots, K-1 \tag{30}$$

The sensor positions $\boldsymbol{\chi}$ and $\boldsymbol{\gamma}$ can be also solved by the LS method as

$$\begin{bmatrix} \hat{\boldsymbol{\chi}} \\ \hat{\boldsymbol{\gamma}} \end{bmatrix} = \left(\boldsymbol{H}^T\boldsymbol{H}\right)^{-1}\boldsymbol{H}^T\boldsymbol{\varsigma} \tag{31}$$

Note that $\hat{y}_1$ will be constrained equal to 0 regardless of the estimation value of $\hat{\boldsymbol{\gamma}}(1)$. Thus, the new sensor positions are obtained.

The final DOAs and sensor positions are estimated by repeating the two steps above till convergence. The proposed method is summarized in Table 1.

4. Algorithm analysis

Herein we discuss certain points relative to the proposed method.

1) *Computational complexity analysis:* The proposed method contains two parts: propagation delays estimation and two-step iteration. The computational complexity of propagation delays estimation is $O(0.5MN_fN_t\log_2 N_t + N_fN_tM + N_s(N_s-1)M)$, where M, N_t, N_f, and N_s denote the number of sensors, the number of TF points at each time-slice, the number of TF points at each frequency-slice, and the number of TF points after noise thresholding, sequentially. The computational complexity of the two-step iteration mainly depends on the calculation of positions in (31). Its computational complexity is $O([8(M-1)^3 + 4(M-1)^3K]N_{iter1})$ with N_{iter1} and K denoting the number of iterations and the number of sources, respectively. Hence the total computational complexity of the proposed algorithm is $O(0.5MN_fN_t\log_2 N_t + N_fN_tM + N_s(N_s-1)M + [8(M-1)^3 + 4(M-1)^3K]N_{iter1})$. In Table 2, we compare the proposed method with other methods, where L, N_θ, N_{iter2}, N_{iter3}, and P denote the number of frequencies, the number of DOA searches, the number of iterations in

Table 2
Computational complexity and run time of algorithms.

Algorithm	Complexity	Run time (s)
Proposed	$O(0.5MN_fN_t\log_2 N_t + N_fN_tM + N_s(N_s-1)M + [8(M-1)^3 + 4(M-1)^3K]N_{iter1})$	3.9544
WF	$O([8M^3 + 4M^2(M-K)KL + N_\theta LM]N_{iter2} + M^3L)$	4.9505
PSO-based	$O((K^3 + 4M^3 + 2M^2)LPN_{iter3})$	161.7614

WF method, the number of iterations in PSO-based method, and the number of initial particles, sequentially. Note that N_{iter3} is much larger than N_{iter1} and N_{iter2} due to the slow convergence rate of PSO-based method. Generally, the proposed algorithm and WF algorithm converge within 50 iterations, while the PSO-based algorithm needs more than 400 iterations. In Table 2, the run time is also given. Herein we run all the methods using MATLAB 2012a on a Windows 7 with dual core 3.4 GHz Intel Core i7 CPU and 7.88 GB memory, and set $M = 9$, $L = 20$, $K = 3$, $N_f = 512$, $N_t = 512$, $N_\theta = 1800$, $N_{iter1} = 50$, $N_{iter2} = 50$, $N_{iter3} = 400$ and $P = 30$. No code optimization is utilized. It can be seen that compared with other self-calibration methods, the proposed one is more efficient.

2) *Condition:* The proposed method is based on the assumption that the sources do not overlap completely in the TF domain, which is easily met in practice [12–20]. If two array signals have the same TFDs, they must share the same frequency components, time of arrival (TOA) and DOA. This condition is extremely restrictive in practice. Even one source and its multipath signals will have different TFDs for different TOAs and DOAs.

3) *TFD selection:* Generally TFD can be classified as linear or quadratic TFD depending on whether it satisfies the linear superposition principle. The quadratic TFD has high resolution, but it has cross-terms and high computational complexity. By contrast, the linear TFD has low resolution, but the cross-term is avoided and the computational complexity is much lower. STFT is a well-known linear TFD. The main intuition of choosing STFT in this paper is that it is simple to implement and the cross-term can be avoided. In fact, the procedure of the self-calibration is much more complex than that of normal DOA estimation. Hence we would choose a simpler TFD.

4) *Underdetermined case:* If there are more sources than sensors, the DOA estimation is underdetermined. The WF method and PSO-based method both require that the number of sources is smaller than the number of sensors. To realize self-calibration, at least three sources are needed, and more calibration sources produce better performance. For small array, it is possible that the sources are more than the sensors, which leads to the ineffectiveness of WF method and PSO-based method. The proposed method can handle this underdetermined case effectively, since it separates the sources one by one and estimates the DOAs separately without using the noise subspace.

Besides, the Cramer–Rao bound (CRB) has been derived in *Section 8.11.2* of [21]. One can refer to it for details.

5. Simulation results

In this part, we first show the calibration results of the proposed method, then compare it with other algorithms.

5.1. Calibration results of the proposed method

The nominal array is a 3×3 uniform square array with 9 sensors $r_0, r_1, \ldots, r_8$ arranged as Fig. 2. The first sensor r_0 is chosen as the reference sensor. Its exact position is known as well as the y position of the sensor r_1. Assuming the sources fall in 0.5 GHz $\sim$ 1.0 GHz, then the nominal inter-sensor spacing Δd is set as the half wavelength $0.5\lambda_{\min}$ corresponding to $f_{\max} = 1.0$ GHz. Three wideband sources s_0, s_1 and s_2 impinge on the array from -45^o, 20^o and 55^o. s_0 and s_1 are linear chirp signal and sinusoidal frequency modulated signal, respectively, with the same frequency range 0.6 GHz $\sim$ 0.9 GHz, and s_2 is a frequency hopping signal with three frequencies 0.62 GHz, 0.75 GHz and 0.83 GHz. The three sources have equal power with 10 dB signal-to-noise ratio (SNR), and the received signals are collected with 512 snapshots for each sensor. The parameters ε_1 and ε_2 are both set as 0.2.

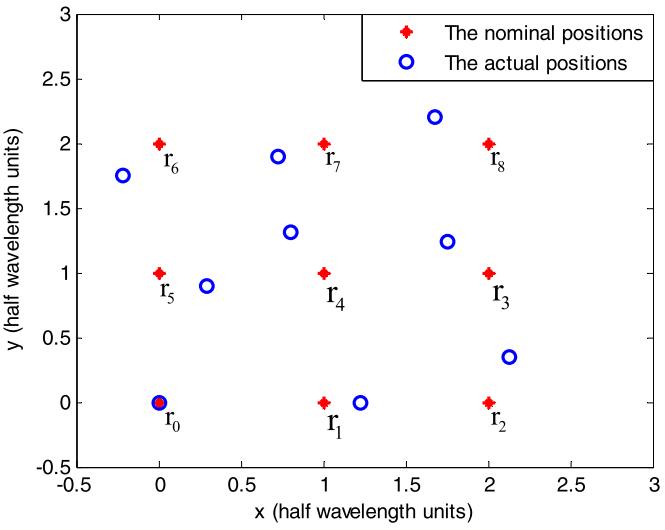

Fig. 2. The actual positions and nominal positions of all the sensors.

Table 3
The actual positions, nominal positions and perturbations (half wavelength Δd).

	Actual positions	Nominal positions	Perturbations
r_0	(0, 0)	(0, 0)	0
r_1	(1.23, 0)	(1, 0)	0.23
r_2	(2.13, 0.35)	(2, 0)	0.3734
r_3	(1.75, 1.24)	(2, 1)	0.3466
r_4	(0.8, 1.31)	(1, 1)	0.3689
r_5	(0.29, 0.9)	(0, 1)	0.3068
r_6	(−0.22, 1.75)	(2, 0)	0.333
r_7	(0.73, 1.9)	(2, 1)	0.2879
r_8	(1.68, 2.2)	(2, 2)	0.3774

Table 3 and Fig. 2 show the actual positions, nominal positions and the corresponding perturbations of all the sensors. To show that the proposed method can achieve good performance even under large position errors, most of the perturbations are set larger than $0.3\Delta d$, with which the DOAs cannot be estimated accurately by WF method. Here the perturbations denote the distance between the nominal positions and the actual positions.

In Fig. 3, the top three plots represent the TFDs of s_0, s_1, and s_2, respectively. We can see the three signals have some overlapping TF points. Fig. 3 (d) shows the 3-D TFDs of the received signals. For convenience, we show the following results with 2-D graph as Fig. 3 (e), which clearly illustrates that the TFDs consist of single-source points, overlapping points and many noise points. The result after noise thresholding procedure is shown in Fig. 3 (f), in which most noise points are removed. Fig. 3 (g)–(i) show the single-source points of s_0, s_1, and s_2 after clustering, respectively. Compared with Fig. 3 (a)–(c), the distributions of the single-source points are fragmentary, since overlapping points are filtered out. However, this has little influence on the estimation of the delay

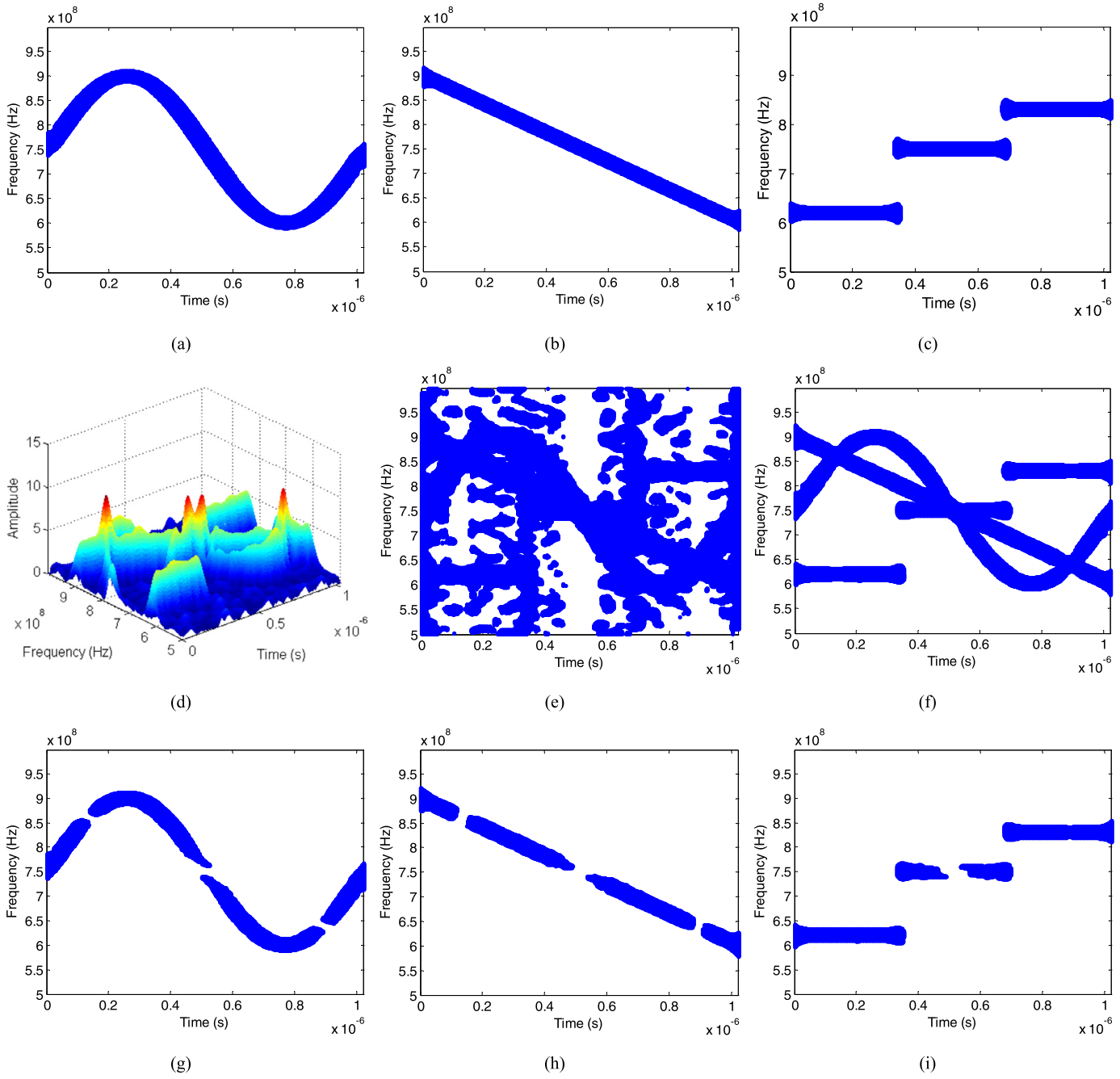

Fig. 3. (a), (b) and (c) represent the TFDs of s_0, s_1, and s_2, respectively. (d) and (e) represent the 3-D and 2-D TFDs of the received signals. (f) represents the TFDs after removing the noise points. (g), (h) and (i) represent single-source points of s_0, s_1, and s_2, respectively.

vector, since the estimation only needs some TF points of each source but not all.

Fig. 4 compares the estimated propagation delays with the actual ones illustrating that the proposed TF method can estimate the propagation delays accurately. With the propagation delays, the sensor positions and DOAs are then estimated by the two-step iteration, and the results are shown in Fig. 5. It can be observed that the estimated positions are very close to the actual ones with slight errors shown in Fig. 5 (a), and the corresponding DOAs estimation also has much better performance than that using the nominal positions shown in Fig. 5 (b). Fig. 6 (a) presents the biases of positions versus iterations for all the sensors, we can see that the biases decrease with the iterations and all the final biases are less than $0.02\Delta d$, some of them are even less than $0.01\Delta d$, which are small enough for DOAs estimation. As expected, the biases of DOAs also decrease with the iterations, and the final biases are 0.3^o, 0.12^o and 0.27^o shown in Fig. 6 (b). From the simulation results above, it can be demonstrated that the proposed method can estimate the sensor positions and DOAs accurately even under large position errors.

5.2. Performance comparison

In this section, we compare the performance of the proposed method with the standard MUSIC method, WF method, PSO-based method, and the CRB. The scenario here is similar to subsection 5.1 except that the perturbations of x and y positions are modeled as independent, identically distributed Gaussian random variables

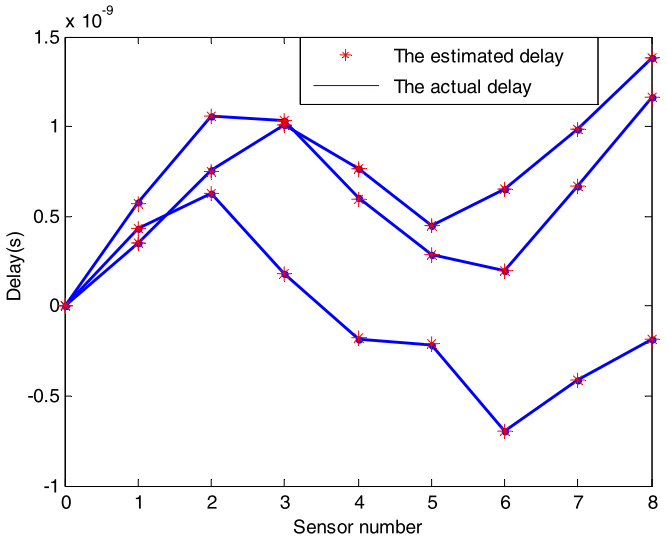

Fig. 4. Comparation between the estimated delay vectors and the actual ones.

with standard deviation δ. The following results are averaged over 200 Monte Carlo runs.

Fig. 7 (a) shows the DOA estimation performance versus SNR, where the standard deviation is set as $\delta = 0.1\Delta d$. It can be seen that the standard MUSIC method fails immediately over the whole SNR range illustrating the serious performance degradation caused by position errors. Compared with MUSIC, the WF method can achieve better performance, but the improvement is finite. By contrast, the proposed method and the PSO-based method can estimate the DOAs accurately, whose mean square errors (MSEs) are always close to the CRB. In Fig. 7 (b), the standard deviation is enlarged to $\delta = 0.3\Delta d$ resulting in worse performances of the MUSIC and WF methods. However, the proposed method and PSO-based method can still remain accurate estimation regardless of larger perturbations. To demonstrate this further, DOA estimation performance versus the standard deviation is given in Fig. 9 (a) with SNR = 20 dB. It can be seen that the DOA MSEs of MUSIC method and WF method deviate quickly from the CRB with the standard deviation increasing, whereas the MSEs of the proposed method and PSO-based method come closest to the CRB over the entire range of pertur-

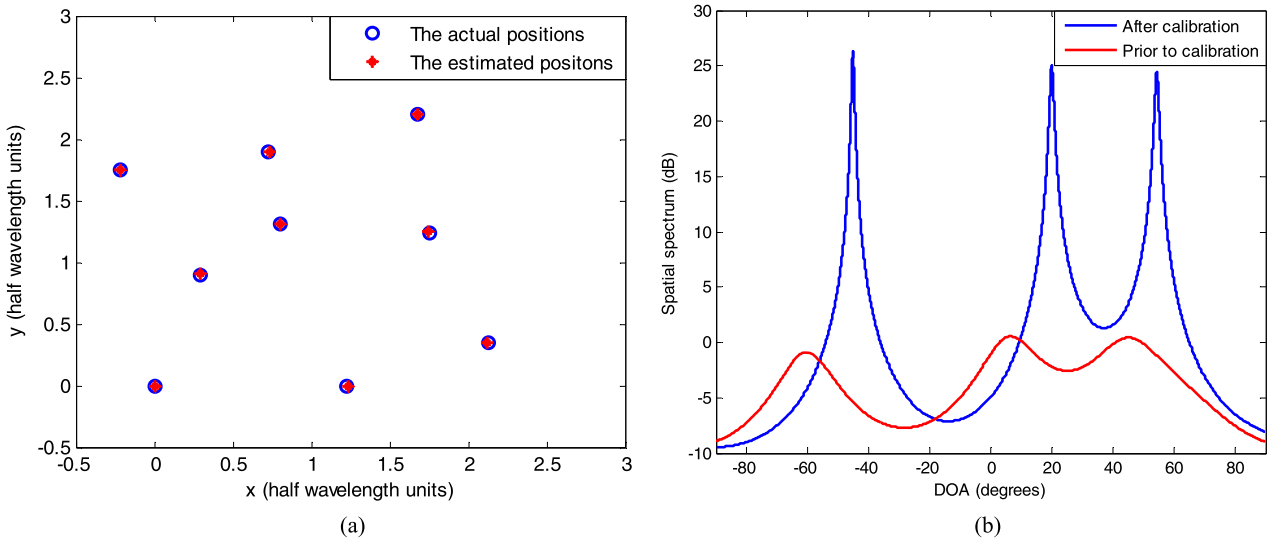

Fig. 5. (a) shows the results of positions estimation. (b) gives the comparation of spatial spectrums between one obtained with the estimated positions and the other with the nominal positions.

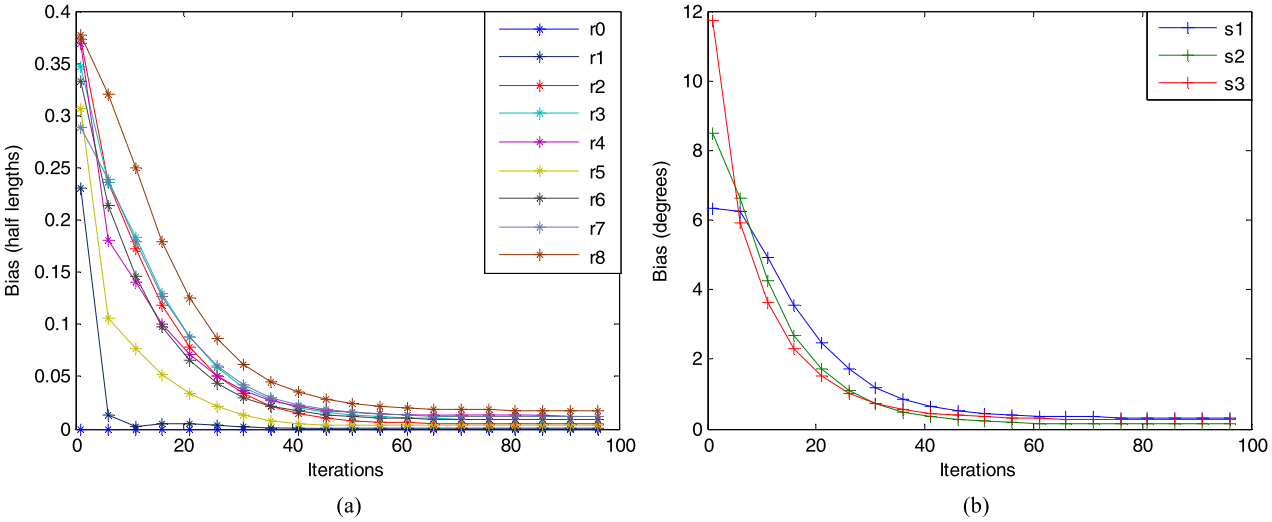

Fig. 6. (a) and (b) present the biases of positions and DOAs versus iterations, respectively.

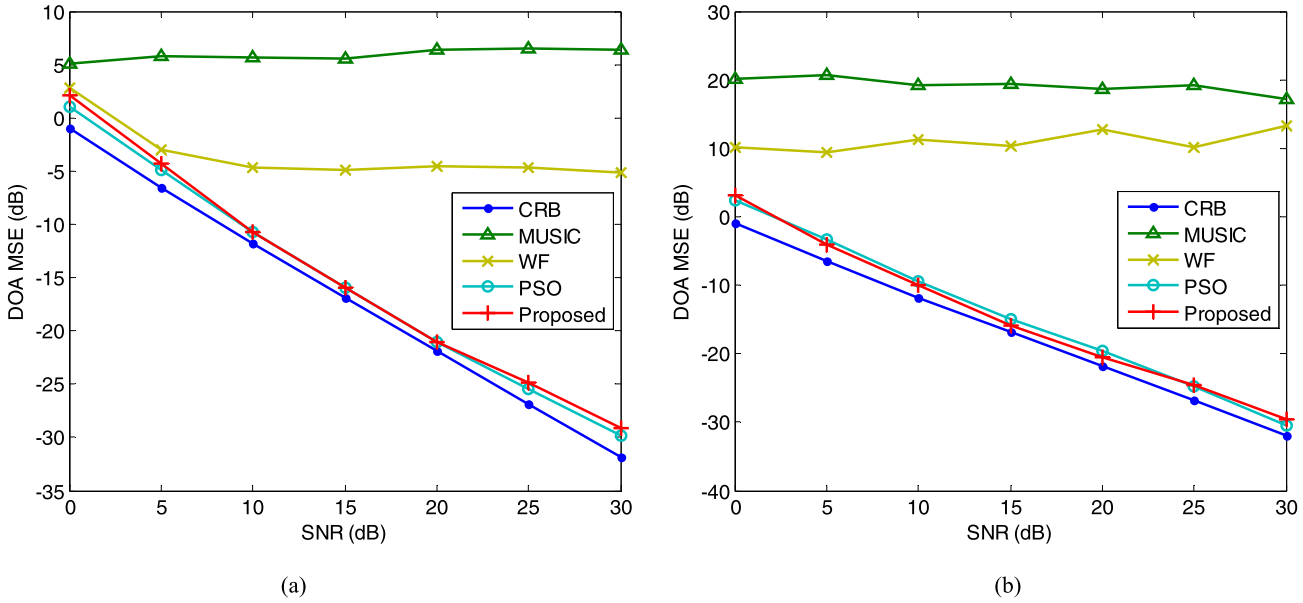

Fig. 7. Comparison of DOA estimation performance versus SNR under small position error as (a) $\delta = 0.1\Delta d$ and large position error as (b) $\delta = 0.3\Delta d$.

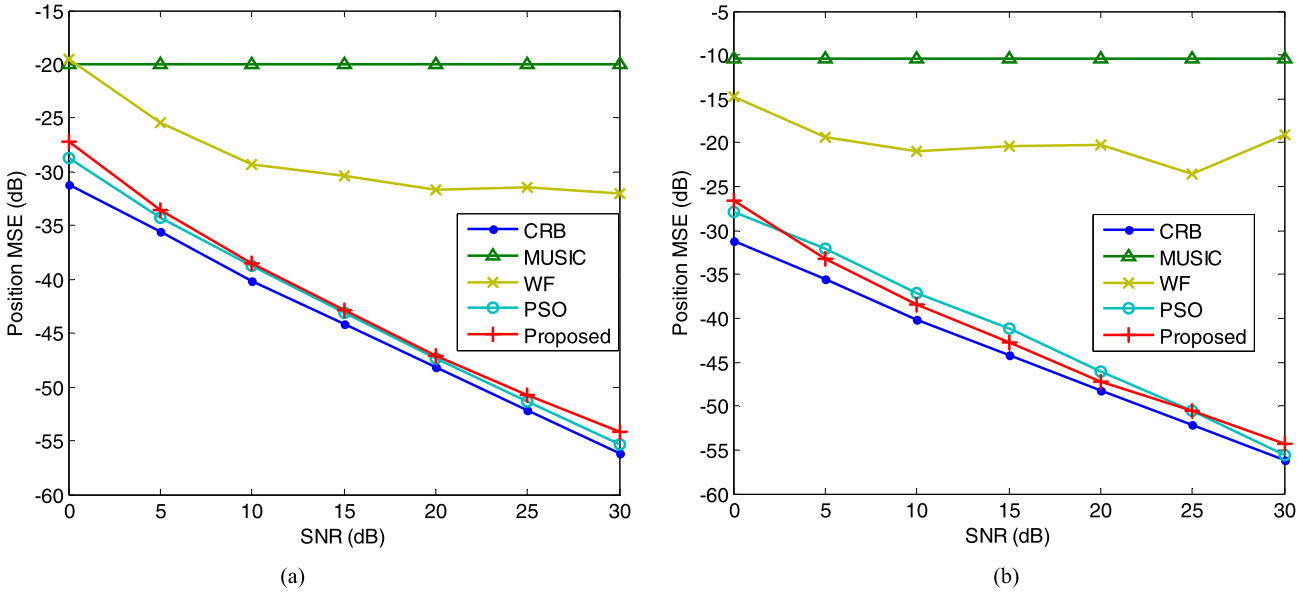

Fig. 8. Comparison of position estimation performance versus SNR under small position error as (a) $\delta = 0.1\Delta d$ and large position error as (b) $\delta = 0.3\Delta d$.

bations. However, the computational complexity of the PSO-based algorithm is much higher than the proposed algorithm shown in Table 2.

Since the DOA estimation and position estimation depend on each other, they have similar performance versus input SNR and standard deviation. Fig. 8 shows the position estimation performance versus input SNR under $\delta = 0.1\Delta d$ and $\delta = 0.3\Delta d$. As expected, the WF method and MUSIC method cannot achieve good enough performance. By contrast, the proposed method and the PSO-based method can calibrate the positions accurately. Fig. 9 (b) gives the position estimation MSE versus standard deviation δ, we can see that the proposed method and PSO-based method can always achieve satisfactory performance. Consequently, it can be verified the proposed method is robust against sensor position errors, and an accurate DOA and position estimation can be always achieved with lower computational complexity.

6. Conclusion

In this paper, a wideband array self-calibration method based on TFDs is proposed, which has robust performance even in the presence of large position errors. We develop an approach to select the single-source points for wideband signals, then calculate the propagation delays using the selected points. The final DOAs and sensor positions are estimated simultaneously by a two-step iteration. Unlike conventional methods, our method does not require any approximation or global optimization, and it has better performance compared to other methods. Simulation results illustrate the effectiveness of the proposed method. Besides, the method can be easily extended to narrowband case and arbitrary arrays.

Appendix A. Supplementary material

Supplementary material related to this article can be found online at https://doi.org/10.1016/j.dsp.2018.03.013.

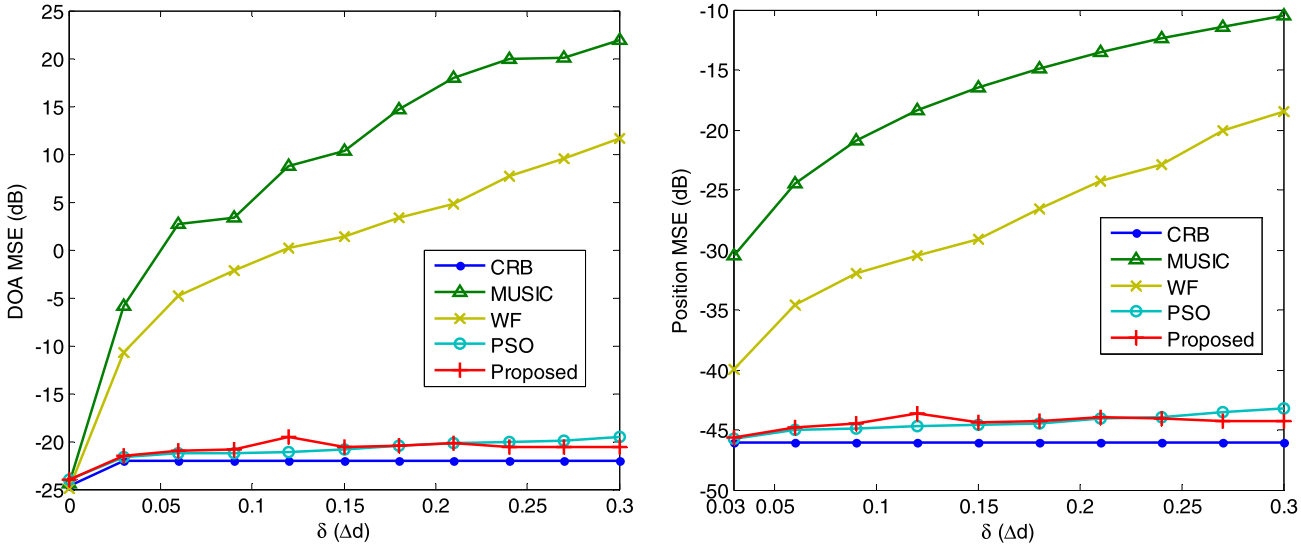

Fig. 9. Comparison of DOA estimation performance (a) and position estimation performance (b) versus the standard deviation with SNR = 20 dB.

References

[1] L. Wang, L.F. Zhao, G.A. Bi, et al., Novel Wideband DOA estimation based on sparse Bayesian learning with Dirichlet process priors, IEEE Trans. Signal Process. 64 (2) (2016) 275–289.

[2] B. Liao, S.C. Chan, L. Huang, et al., Iterative methods for subspace and DOA estimation in nonuniform noise, IEEE Trans. Signal Process. 64 (12) (2016) 3008–3020.

[3] R. Long, J. Ouyang, F. Yang, et al., Fast amplitude-only measurement method for phased array calibration, IEEE Trans. Antennas Propag. 65 (4) (2017) 1815–1821.

[4] A.M. Elbir, Calibration of directional mutual coupling for antenna arrays, Digit. Signal Process. 69 (2017) 117–126.

[5] E. BouDaher, F. Ahmad, M.G. Amin, et al., Mutual coupling effect and compensation in non-uniform arrays for direction-of-arrival estimation, Digit. Signal Process. 61 (2017) 3–14.

[6] S. Wan, J. Tang, W. Zhu, N. Zhang, Identifiability analysis for array shape self-calibration based on Hybrid Cramér–Rao bound, IEEE Signal Process. Lett. 21 (4) (2014) 473–477.

[7] Y. Rockah, P.M. Schultheiss, Array shape calibration using sources in unknown locations – part I: far-field sources, IEEE Trans. Acoust. Speech Signal Process. 35 (3) (1987) 286–299.

[8] A.J. Weiss, B. Friedlander, Array shape calibration using sources in unknown locations – a maximum likelihood approach, IEEE Trans. Acoust. Speech Signal Process. 37 (12) (1989) 1958–1966.

[9] A.J. Weiss, B. Friedlander, Array shape calibration using eigenstructure methods, Signal Process. 22 (3) (1991) 251–258.

[10] B.P. Flanagan, K.L. Bell, Array self-calibration with large sensor position errors, Signal Process. 81 (10) (2001) 2201–2214.

[11] S. Wan, P.J. Chung, B. Mulgrew, Maximum likelihood array calibration using particle swarm optimisation, IET Signal Process. 6 (5) (2012) 456–465.

[12] F. Abrard, Y. Deville, A time-frequency blind signal separation method applicable to underdetermined mixtures of dependent sources, Signal Process. 85 (7) (2005) 1389–1403.

[13] Y.H. Luo, W.W. Wang, J.A. Chambers, et al., Exploitation of source nonstationarity in underdetermined blind source separation with advanced clustering techniques, IEEE Trans. Signal Process. 54 (6) (2006) 2198–2212.

[14] A. Aïssa-El-Bey, N. Linh-Trung, K. Abed-Meraim, et al., Underdetermind blind separation of nondisjoint sources in the time-frequency domain, IEEE Trans. Signal Process. 55 (3) (2007) 897–907.

[15] D.Z. Peng, Y. Xiang, Underdetermined blind source separation based on relaxed sparsity condition of sources, IEEE Trans. Signal Process. 57 (2) (2009) 809–814.

[16] M. Amin, Y. Zhang, Direction finding based on spatial time-frequency distribution matrices, Digit. Signal Process. 10 (4) (2000) 325–339.

[17] S. Ghofrani, M.G. Amin, Y.D. Zhang, High-resolution direction finding of non-stationary signals using matching pursuit, Signal Process. 93 (12) (2013) 3466–3478.

[18] H.J. Zhang, G.L. Bi, Y.L. Cai, et al., DOA estimation of closely-spaced and spectrally-overlapped sources using a STFT-based MUSIC algorithm, Digit. Signal Process. 52 (2016) 25–34.

[19] O. Cholnam, K. Dokkil, J. Cholyong, Spatial spectrum for direction of arrival estimation of multiple non-stationary wideband sources in the time-frequency plane, IET Signal Process. 10 (9) (2016) 1105–1111.

[20] A.B. Gershman, M.G. Amin, Wideband direction-of-arrival estimation of multiple chirp signals using spatial time-frequency distributions, IEEE Signal Process. Lett. 7 (6) (2000) 152–155.

[21] H.L. Van Trees, Optimum Array Processing, Wiley-Interscience, New York, 2002.

Yaqi Liu received his B.Eng. and M.S. degrees both from National Digital Switching System Engineering and Technological Research Center (NDSC), Zhengzhou, China, in 2012 and 2015; respectively. He is currently working toward Ph.D. degree in NDSC. His research interests include array signal processing and radar signal processing.

Chengcheng Liu received the B.Eng., M.S., and Ph.D. degrees from NDSC, Zhengzhou, China, in 2006, 2011, and 2014; respectively. At present, he is a lecturer in NDSC. His research interests include array signal processing, wireless sensor network, and wireless communications.

Yongjun Zhao received the M.S. and Ph.D. degrees from Beijing institute of Technology, Beijing, China, in 1993 and 2008, respectively. He is currently a professor in NDSC. His current research interests include radar signal processing, array signal processing, and source localization.

Jiandong Zhu received the B.Eng., M.S., and Ph.D. degrees from NDSC, Zhengzhou, China, in 2003, 2006, and 2013; respectively. At present, he is a researcher in Electronic Equipment Test Center, Luoyang, China. His research interests include wireless communications and radar parameter estimation.